Dark matter spin effects

Bohdan GRZADKOWSKI
University of Warsaw

- The goal
- Pseudo-Goldstone dark matter (pGDM)
- Vector dark matter (VDM)
- Fermion dark matter (FDM)
- Parameters
- Constraints
- Dark matter at e^+e^- colliders
- Summary

◇ BG, M.Iglicki, K.Mekala and A. F.Zarnecki, "Dark-matter-spin effects at future e^+e^- colliders", JHEP 08 (2020) 052, e-Print: 2003.06719 ,

◇ D.Azevedo, M.Duch, BG, D.Huang, M.Iglicki, R.Santos, "One-loop contribution to dark matter-nucleon scattering in the pseudoscalar dark matter model", JHEP 1901 (2019) 138,

◇ D.Azevedo, M.Duch, BG, D.Huang, M.Iglicki, R.Santos, "Testing scalar versus vector dark matter", Phys.Rev. D99 (2019) no.1, 015017,

◇ M.Duch, BG, M.McGarrie, "A stable Higgs portal with vector dark matter", JHEP 1509 (2015) 162

The goal

- Find simple (not simplified) consistent and renormaizable models of Dark Mater (DM) of spin 0, $1/2$ and 1.
- Impose experimental and theoretical constraints.
- Maximize signals and differences between cross-sections to compare the models in a meaningful way.

Pseudo-Goldstone Dark Matter (pGDM)

- J. Cline, T. Toma, "Pseudo-Goldstone dark matter confronts cosmic ray and collider anomalies", Phys.Rev.D 100 (2019) no.3, 035023,
- D. Karamitros, "Pseudo Nambu-Goldstone Dark Matter: Examples of Vanishing Direct Detection Cross Section", Phys.Rev. D99 (2019) no.9, 095036,
- K. Kannike, M. Raidal, "Phase Transitions and Gravitational Wave Tests of Pseudo-Goldstone Dark Matter in the Softly Broken $U(1)$ Scalar Singlet Model", Phys.Rev. D99 (2019) no.11, 115010,
- T. Alanne, M. Heikinheimo, V. Keus, N. Koivunen, K. Tuominen, "Direct and indirect probes of Goldstone dark matter", Phys.Rev. D99 (2019) no.7, 075028,
- K Huitu, N. Koivunen, O. Lebedev, S. Mondal, T. Toma, "Probing pseudo-Goldstone dark matter at the LHC", arXiv:1812.05952,
- K. Ghorbani, P. Hossein Ghorbani, "Leading Loop Effects in Pseudoscalar-Higgs Portal Dark Matter", JHEP 1905 (2019) 096,
- K. Ishiwata, T. Toma, "Probing pseudo Nambu-Goldstone boson dark matter at loop level", JHEP 1812 (2018) 089,
- D. Azevedo, M. Duch, BG, D. Huang, M. Iglicki, R. Santos, "One-loop contribution to dark matter-nucleon scattering in the pseudoscalar dark matter model", JHEP 1901 (2019) 138,
- D. Azevedo, M. Duch, BG, D. Huang, M. Iglicki, R. Santos, "Testing scalar versus vector dark matter", Phys.Rev. D99 (2019) no.1, 015017,
- C. Gross, O. Lebedev, and T. Toma, "Cancellation Mechanism for Dark-Matter–Nucleon Interaction", Phys. Rev. Lett. 119 (2017), no. 19 191801.

$$V_{\text{pGDM}}(H,S) = -\mu_H^2|H|^2 + \lambda_H|H|^4 - \mu_S^2|S|^2 + \lambda_S|S|^4 + \kappa|S|^2|H|^2 + (\mu^2 S^2 + \text{H.c.})$$

$$S = \frac{1}{\sqrt{2}}(v_S + \phi + iA) \quad , \quad \text{and} \quad H = \begin{pmatrix} \pi^+ \\ \frac{1}{\sqrt{2}}(v + h + i\pi^0) \end{pmatrix}.$$

Positivity: $\lambda_H > 0, \quad \lambda_S > 0, \quad \kappa > -2\sqrt{\lambda_H \lambda_S}$

Symmetries:

- $\mu^2 \neq 0$ breaks global $U(1)$ softly to residual $Z_2 : S \to -S$,
- rephase S such that $\text{Im}\,\mu^2 = 0$ (basis choice),
- $V \ni \mu^2(S^2 + S^{*\,2})$, so $S \xrightarrow{C} S^*$ ($\phi \to \phi$ and $A \to -A$) is a symmetry,
- global minimum at $\langle S \rangle = \frac{v_S}{\sqrt{2}}$ with v_S being real, so C is unbroken and A is a stable DM candidate, $m_A^2 \propto \mu^2$, if $\mu^2 \to 0$ then A becomes a Goldstone boson of broken $U(1)$,

$$S = \frac{1}{\sqrt{2}}(v_S + \phi + iA) \quad , \quad \text{and} \quad H = \begin{pmatrix} \pi^+ \\ \frac{1}{\sqrt{2}}(v + h + i\pi^0) \end{pmatrix}.$$

$$\mathcal{M}^2 = \begin{pmatrix} 2\lambda_H v^2 & \kappa v v_S & 0 \\ \kappa v v_S & 2\lambda_S v_S^2 & 0 \\ 0 & 0 & -4\mu^2 \end{pmatrix}$$

$$\mathcal{M}^2_{\text{diag}} = \begin{pmatrix} m_1^2 & 0 & 0 \\ 0 & m_2^2 & 0 \\ 0 & 0 & m_A^2 \end{pmatrix}, \quad R = \begin{pmatrix} \cos\alpha & -\sin\alpha \\ \sin\alpha & \cos\alpha \end{pmatrix}, \quad \begin{pmatrix} h_1 \\ h_2 \end{pmatrix} = R^{-1} \begin{pmatrix} h \\ \phi \end{pmatrix},$$

$$V_{\text{pGDM}} \ni \lambda_S |S|^4 + \kappa |S|^2 |H|^2 \ni \frac{A^2}{2}(2\lambda_S v_S \phi + \kappa v \phi) = \frac{A^2}{2v_S}(\sin\alpha\, m_1^2 h_1 + \cos\alpha\, m_2^2 h_2)$$

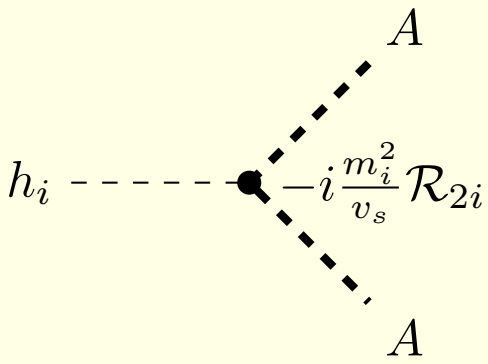

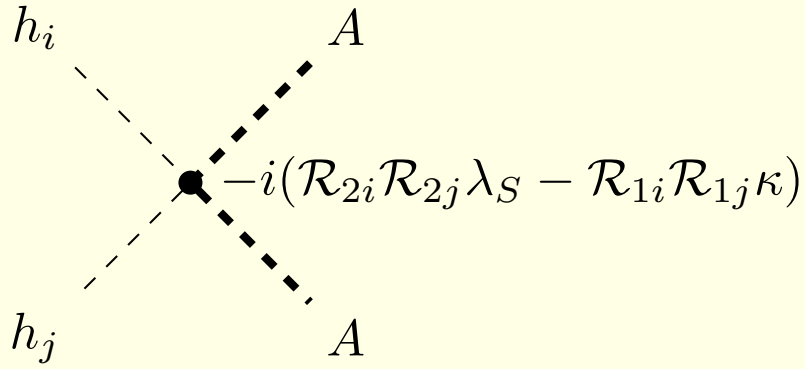

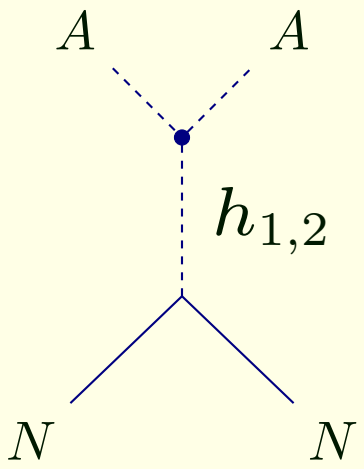

The DM direct detection signals are naturally suppressed in the pGDM model:

$$
\begin{aligned}
i\mathcal{M} &= -i\frac{\sin\alpha\cos\alpha f_N m_N}{v v_S}\left(\frac{m_1^2}{q^2-m_1^2}-\frac{m_2^2}{q^2-m_2^2}\right)\bar{u}_N(p_4)u_N(p_2) \\
&\approx -i\frac{\sin\alpha\cos\alpha f_N m_N}{v v_S}\left(\frac{m_1^2-m_2^2}{m_1^2 m_2^2}\right)q^2\bar{u}_N(p_4)u_N(p_2)\,.
\end{aligned}
$$

The total cross section σ_{AN}:

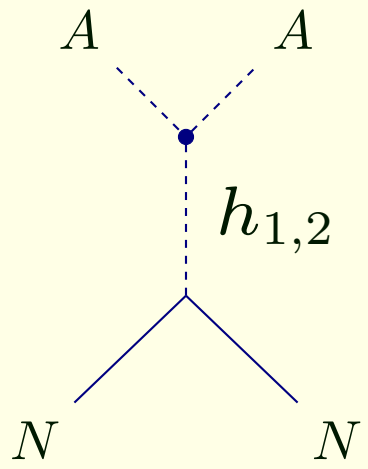

$$\sigma_{AN}^{(tree)} \propto \frac{\sin^2\alpha\cos^2\alpha}{v_S^2}(m_1^2 - m_2^2)^2 \times v_A^4\,,$$

where v_A is the A velocity in the lab frame. Since $v_A \sim 200$ km/s, the total DM nuclear recoil cross section σ_{AN} is greatly suppressed by the factor $v_A^4 \sim 10^{-13}$:

$$\sigma_{AN}^{(tree)} \sim 10^{-70}\ \text{cm}^2 \ll \sigma_{AN}^{(\text{X}ENON1T)} \sim 10^{-46}\ \text{cm}^2$$

$$\Downarrow$$

1-loop effects are leading

- if $q^2 \to 0$ then loop corrections are expected to be UV finite,
- if $m_A^2 \propto \mu^2 \to 0$ then loop corrections should vanish.

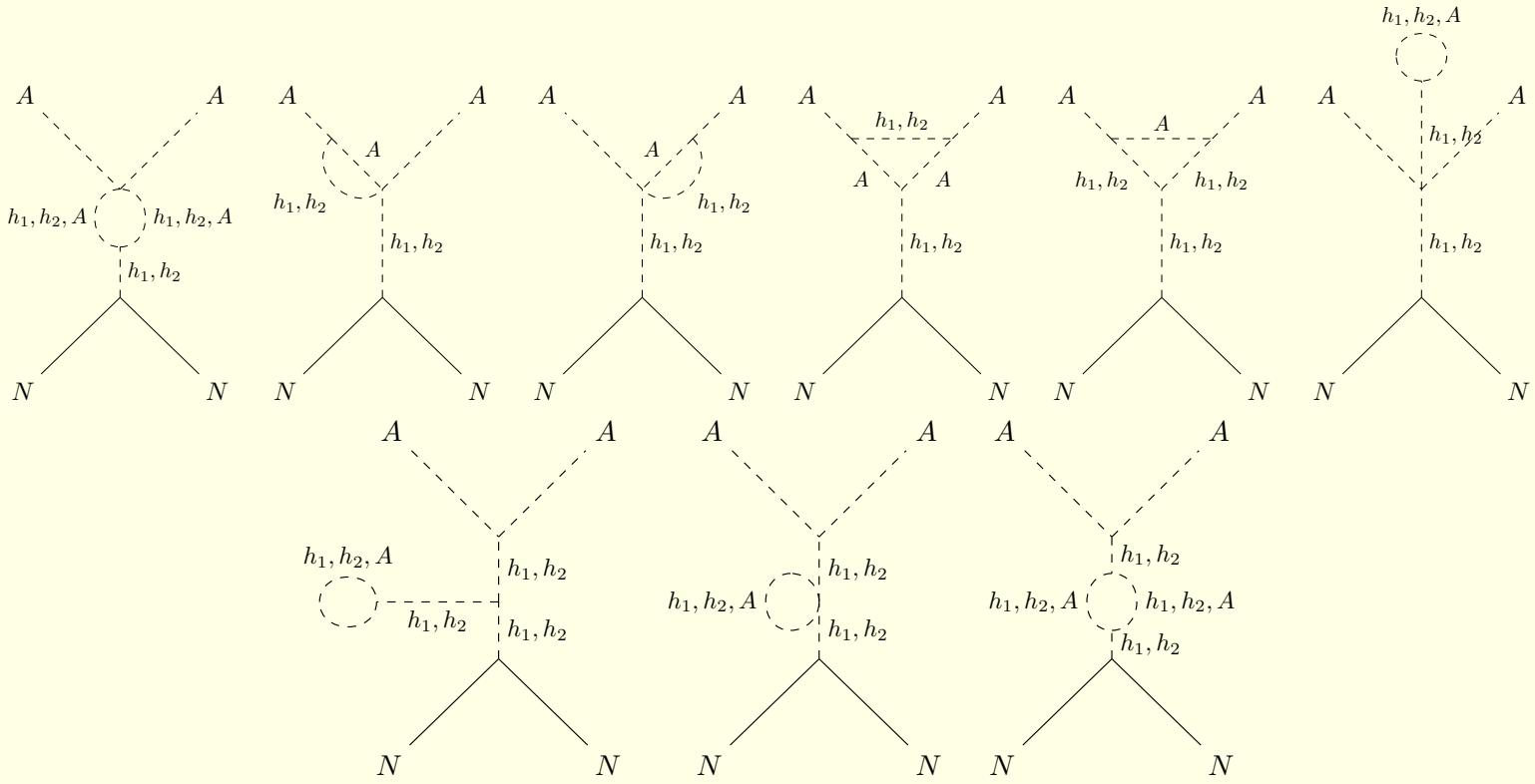

Figure 1: 1-loop diagrams contributing to A-nucleon scattering.

$$\sigma_{AN}^{(1)} = \frac{f_N^2}{\pi v^2} \frac{m_N^2 \mu_{AN}^2}{m_A^2} \mathcal{F}^2 \,,$$

where the one-loop function $\mathcal{F}$ is defined as

$$\mathcal{F} = \frac{V_{AA1}^{(1)} c_\alpha}{m_1^2} - \frac{V_{AA2}^{(1)} s_\alpha}{m_2^2}$$

with $V_{AA1\,,AA2}^{(1)}$ as one-loop corrections to the vertices $h_1 A^2$ and $h_2 A^2$.

$$\sigma_{\mathsf{AN}} = \frac{\mu^2 m_{\mathsf{DM}}^2}{\pi} \cdot \frac{m_N^2}{v^2} \frac{f_N^2}{m_1^4 m_2^4} \cdot \frac{\sin^2\alpha \cos^2\alpha}{v_S^2} (m_1^2 - m_2^2)^2 \cdot \left[\frac{\mathcal{A}}{64\pi^2 v v_S^2}\right]^2 ,$$

$$\begin{aligned}\mathcal{A} =& a_1 \cdot C_2(0, m_{\mathsf{DM}}^2, m_{\mathsf{DM}}^2, m_1^2, m_2^2, m_{\mathsf{DM}}^2) + \\ & a_2 \cdot D_3(0, 0, m_{\mathsf{DM}}^2, m_{\mathsf{DM}}^2, 0, m_{\mathsf{DM}}^2, m_1^2, m_1^2, m_2^2, m_{\mathsf{DM}}^2) + \\ & a_3 \cdot D_3(0, 0, m_{\mathsf{DM}}^2, m_{\mathsf{DM}}^2, 0, m_{\mathsf{DM}}^2, m_1^2, m_2^2, m_2^2, m_{\mathsf{DM}}^2)\end{aligned}$$

with $a_{1,2,3}$ being coefficients
Comments:

- The one loop amplitude $\mathcal{F}$ is UV finite in the limit of zero momentum transfer $q^2 \to 0$,
- $\mathcal{F} \to 0$ for $m_A \to 0$,
- $$V \supset \frac{M^3}{\sqrt{2}}(S + S^*) + \mu^2(S^2 + S^{*2})$$
$$\mathcal{L}_A \supset \frac{1}{2}(\partial^\mu A \partial_\mu A - m_A^2 A^2) - \frac{R_{2i}}{2v_s}\left(m_i^2 + \frac{M^3}{v_S}\right) h_i A^2 .$$

The Vector Dark Matter (VDM) model

- T. Hambye, "Hidden vector dark matter", JHEP 0901 (2009) 028,
- O. Lebedev, H. M. Lee, and Y. Mambrini, "Vector Higgs-portal dark matter and the invisible Higgs", Phys.Lett. B707 (2012) 570,
- Y. Farzan and A. R. Akbarieh, "VDM: A model for Vector Dark Matter", JCAP 1210 (2012) 026,
- S. Baek, P. Ko, W.-I. Park, and E. Senaha, "Higgs Portal Vector Dark Matter : Revisited", JHEP 1305 (2013) 036,
- Ch. Gross, O. Lebedev, Y. Mambrini, "Non-Abelian gauge fields as dark matter", arXiv:1505.07480,
- ...

The model:

- extra $U(1)_X$ gauge symmetry (A^μ_X), DM candidate: A^μ_X,
- a complex scalar field S, whose vev generates a mass for the $U(1)$'s vector field, $S = (0, \mathbf{1}, \mathbf{1}, 1)$ under $U(1)_Y \times SU(2)_L \times SU(3)_c \times U(1)_X$.
- SM fields neutral under $U(1)_X$,
- in order to ensure stability of the new vector boson a $\mathbb{Z}_2$ symmetry is assumed to forbid $U(1)$-kinetic mixing between $U(1)_X$ and $U(1)_Y$. The extra gauge boson A_μ and the scalar S transform under $\mathbb{Z}_2$ (dark charge conjugation) as follows

$$A^\mu_X \xrightarrow{C} -A^\mu_X \ , \ S \xrightarrow{C} S^*$$

The scalar potential

$$V_{\text{VDM}}(H, S) = -\mu_H^2|H|^2 + \lambda_H|H|^4 - \mu_S^2|S|^2 + \lambda_S|S|^4 + \kappa|S|^2|H|^2.$$

For $\kappa^2 < 4\lambda_H\lambda_S$ the global minimum is

$$v^2 = \frac{4\lambda_S\mu_H^2 - 2\kappa\mu_S^2}{4\lambda_H\lambda_S - \kappa^2} \quad \text{and} \quad v_S^2 = \frac{4\lambda_H\mu_S^2 - 2\kappa\mu_H^2}{4\lambda_H\lambda_S - \kappa^2}$$

The mass squared matrix $\mathcal{M}^2$ for the fluctuations (h, ϕ) and their eigenvalues read

$$\mathcal{M}^2 = \begin{pmatrix} 2\lambda_H v^2 & \kappa v v_S \\ \kappa v v_S & 2\lambda_S v_S^2 \end{pmatrix}$$

$$m_\pm^2 = \lambda_H v^2 + \lambda_S v_S^2 \pm \sqrt{\lambda_S^2 v_S^4 - 2\lambda_H\lambda_S v^2 v_S^2 + \lambda_H^2 v^4 + \kappa^2 v^2 v_S^4}$$

$$\mathcal{M}^2_{\text{diag}} = \begin{pmatrix} m_1^2 & 0 \\ 0 & m_2^2 \end{pmatrix}, \quad R = \begin{pmatrix} \cos\alpha & -\sin\alpha \\ \sin\alpha & \cos\alpha \end{pmatrix}, \quad \begin{pmatrix} h_1 \\ h_2 \end{pmatrix} = R^{-1} \begin{pmatrix} h \\ \phi \end{pmatrix},$$

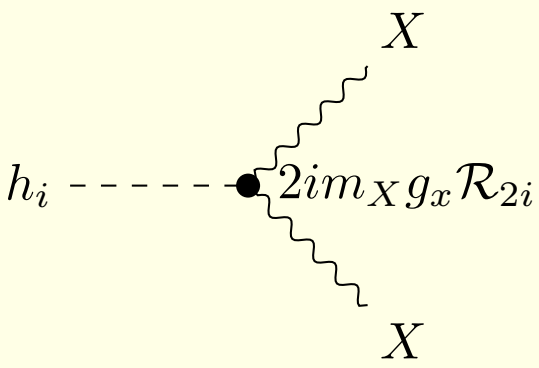

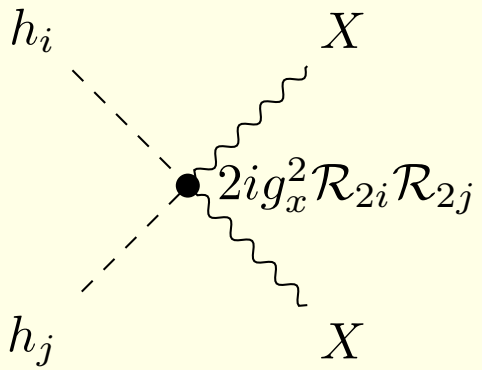

Fermion Dark Matter (FDM)

- DM: χ - a left-handed Dirac fermion,
- spin 0 mediator: S - a real field.

$$\mathbb{Z}_4 : S \to -S \, , \chi \to i\chi$$

$$\begin{aligned} \mathcal{L} &= \mathcal{L}_{\text{SM}} + i\bar{\chi}\partial\!\!\!/\chi + \frac{1}{2}\partial^\mu S \, \partial_\mu S - \frac{y_x}{2}(\bar{\chi^c}\chi + \bar{\chi}\chi^c)S - V(H,S) \, , \\ V_{\text{FDM}}(H,S) &= -\mu_H^2|H|^2 + \lambda_H|H|^4 - \frac{\mu_S^2}{2}S^2 + \frac{\lambda_S}{4}S^4 + \frac{\kappa}{2}|H|^2S^2 \, , \end{aligned}$$

where $\chi^c \equiv -i\gamma_2\chi^*$ and

$$S = v_S + \phi \, , \quad H = \begin{pmatrix} \pi^+ \\ \frac{v+h+i\pi^0}{\sqrt{2}} \end{pmatrix}$$

After SSB relevant parts of the Lagrangian take the following form:

$$i\bar{\chi}\partial\!\!\!/\chi + \frac{1}{2}\partial^\mu S\,\partial_\mu S - \frac{y_x}{2}(\bar{\chi^c}\chi + \bar{\chi}\chi^c)S \to \frac{i}{2}\bar{\psi}\partial\!\!\!/\psi + \frac{1}{2}\partial^\mu\phi\,\partial_\mu\phi - \frac{y_x v_S}{2}\bar{\psi}\psi - \frac{y_x}{2}\bar{\psi}\psi\phi$$

where $\psi = \psi^c \equiv \chi + \chi^c$ is a Majorana mass eigenstate with $m_\psi = y_x v_S$.

$$\begin{pmatrix} h_1 \\ h_2 \end{pmatrix} = \mathcal{R}^{-1}\begin{pmatrix} h \\ \phi \end{pmatrix}\ , \mathcal{R} = \begin{bmatrix} \cos\alpha & -\sin\alpha \\ \sin\alpha & \cos\alpha \end{bmatrix}\ , \alpha \in \left[-\frac{\pi}{4}, \frac{\pi}{4}\right]\ , \tan 2\alpha = \frac{\kappa v v_S}{\lambda_H v^2 - \lambda_S v_S^2}\ .$$

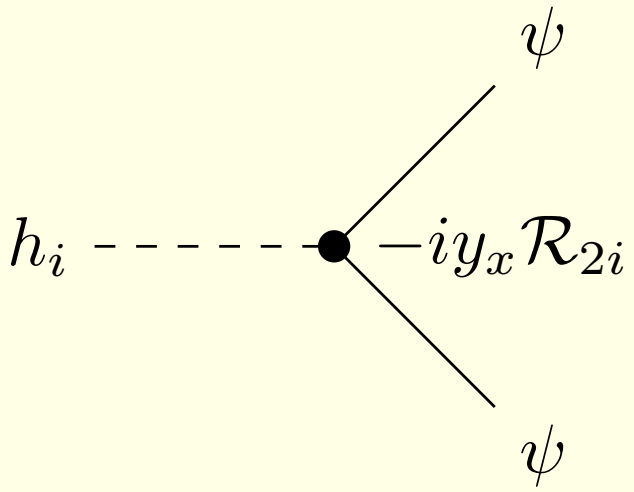

Figure 2: The vertex relevant for the FDM model.

Parameters

$$
\begin{aligned}
V_{\text{pGDM}}(H,S) &= -\mu_H^2|H|^2+\lambda_H|H|^4-\mu_S^2|S|^2+\lambda_S|S|^4+\kappa|S|^2|H|^2+(\mu^2S^2+\text{H.c.})\\
V_{\text{VDM}}(H,S) &= -\mu_H^2|H|^2+\lambda_H|H|^4-\mu_S^2|S|^2+\lambda_S|S|^4+\kappa|S|^2|H|^2\\
V_{\text{FDM}}(H,S) &= -\mu_H^2|H|^2+\lambda_H|H|^4-\frac{\mu_S^2}{2}S^2+\frac{\lambda_S}{4}S^4+\frac{\kappa}{2}|H|^2S^2
\end{aligned}
$$

$$
S=v_S+\phi\ (+iA)\ ,\quad H=\begin{pmatrix}\pi^+\\ \frac{v+h+i\pi^0}{\sqrt{2}}\end{pmatrix}
$$

$$
\begin{pmatrix}h_1\\ h_2\end{pmatrix}=\mathcal{R}^{-1}\begin{pmatrix}h\\ \phi\end{pmatrix}\ ,\mathcal{R}=\begin{bmatrix}\cos\alpha & -\sin\alpha\\ \sin\alpha & \cos\alpha\end{bmatrix}
$$

It is convenient to use the same input parameters for all the models:

$$
m_2,\ \ \sin\alpha,\ \ m_{DM}\equiv(m_A,m_X,m_\psi)\quad\text{and}\quad v_S
$$

- ILC: $\sqrt{s}=250$ GeV $\implies$ $m_{DM}\lesssim 77.5$ GeV

Constraints

1. Perturbativity: $y_x < 4\pi \left(\frac{m_\psi}{v_S} < 4\pi\right)$, $g_X < 4\pi \left(\frac{m_X}{v_S} < 4\pi\right)$, $\kappa < 4\pi$, $\frac{m_i}{v_S} < 4\pi$,

2. Vacuum stability,

3. Minimum globality,

4. Higgs invisible decays (1809.05937):

$$\mathrm{BR}(h_1 \to \mathrm{inv}) = \mathrm{BR}(h_1 \to DM\, DM) < 19\%$$

5. The mixing angle: $0 < \sin\alpha < 0.3$ (1501.02234, 1604.04552).

6. The Planck data (1807.06209): $h^2\,\Omega_{DM} = 0.12 \pm 0.0012$. The thermally averaged cross section ($DM\ DM \to \bar{f} f$) reads:

$$\langle \sigma v \rangle = \frac{n_c}{3}\frac{m_{\mathsf{DM}} m_f^2}{\pi v^2} \cdot \frac{\sin^2\alpha\cos^2\alpha}{v_S^2}(m_1^2 - m_2^2)^2 \cdot \frac{\cdot\left(m_{\mathsf{DM}}^2 - m_f^2\right)^{3/2}}{(4m_{\mathsf{DM}}^2 - m_1^2)^2(4m_{\mathsf{DM}}^2 - m_2^2)^2}\cdot$$

$$\times \begin{cases} 12 + \mathcal{O}\left[\left(\frac{m_{\mathsf{DM}}}{T}\right)^{-1}\right] & (\mathsf{pGDM}) \\ 1 + \mathcal{O}\left[\left(\frac{m_{\mathsf{DM}}}{T}\right)^{-1}\right] & (\mathsf{VDM}) \\ \frac{9}{4}\left(\frac{m_{\mathsf{DM}}}{T}\right)^{-1} + \mathcal{O}\left[\left(\frac{m_{\mathsf{DM}}}{T}\right)^{-2}\right] & (\mathsf{FDM}) \end{cases}$$

$$\langle \sigma v \rangle = \sigma_0 x^{-n} \implies h^2\Omega_{DM} \propto \frac{(n+1)x_f^{n+1}}{\sigma_0} \quad (x \equiv \frac{m_{DM}}{T})$$

$$\Downarrow$$

$$\frac{\sin^2\alpha\cos^2\alpha}{v_S^2}(m_1^2 - m_2^2)^2 =$$

$$= 2.1 \cdot 10^{-5}\ \mathsf{GeV}^{-2}\frac{(4m_{\mathsf{DM}}^2 - m_1^2)^2\,(4m_{\mathsf{DM}}^2 - m_2^2)^2}{m_{\mathsf{DM}}(m_{\mathsf{DM}}^2 - m_b^2)^{3/2}} \cdot \begin{cases} \frac{1}{12} & (\mathsf{pGDM}) \\ 1 & (\mathsf{VDM}) \\ \frac{4m_{DM}}{9T_f} & (\mathsf{FDM}) \end{cases}$$

7. Indirect-detection (1611.03184) limits.

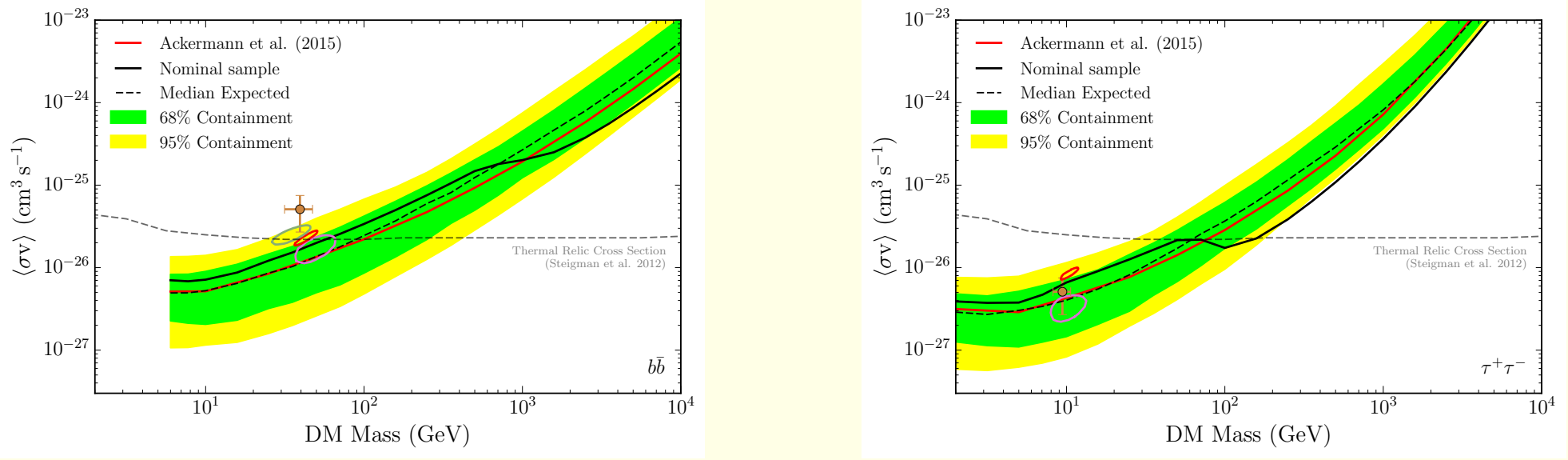

Figure 3: Relic-density and indirect-detection limits. (1611.03184)

- For pGDM and VDM: $m_A, m_X \gtrsim 30$ GeV, since otherwise the proper value of annihilation cross section is forbidden.
- For FDM due to the T_0/T_f factor, current annihilation cross-section corresponding to the correct value of relic density is orders of magnitude times smaller than the one for the pGDM and VDM, hence it satisfies the ID limit.

8. Direct-detecion (1805.12562) constraint the spin-independent nucleon-scattering cross section.

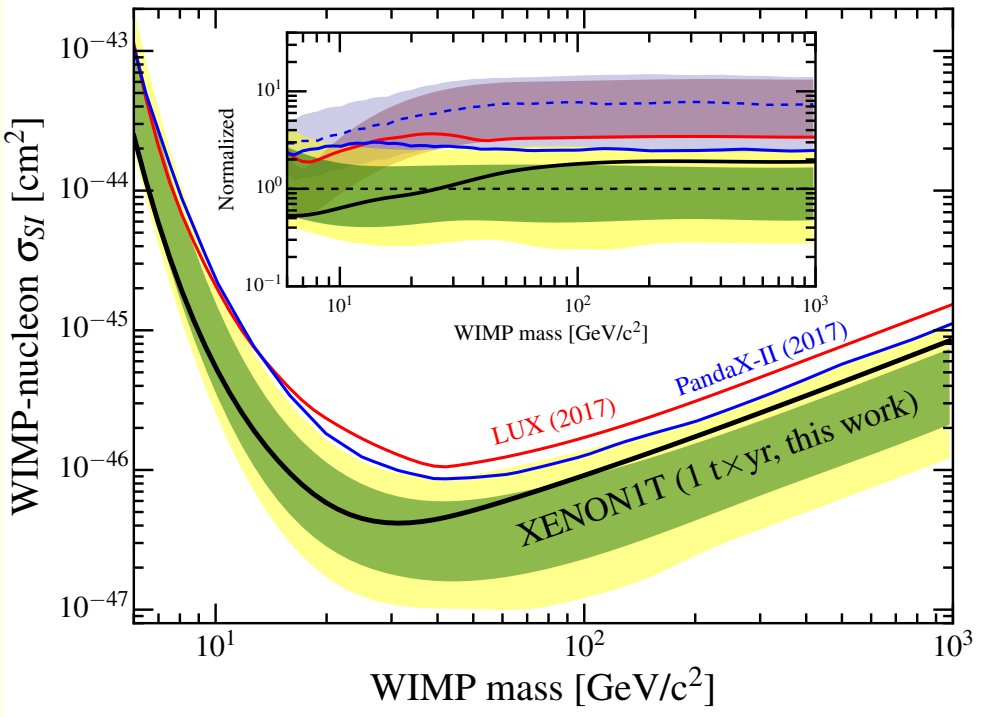

Figure 4: Direct-detection limits. (1805.12562)

For VDM and FDM:

$$\sigma_{\mathsf{SI}} \simeq \frac{\mu^2 m_{\mathsf{DM}}^2}{\pi} \cdot \frac{m_N^2}{v^2} \frac{f_N^2}{m_1^4 m_2^4} \cdot \frac{\sin^2\alpha \cos^2\alpha}{v_S^2} (m_1^2 - m_2^2)^2 \ ,$$

For pGDM 1-loop calculations are needed (1810.06105).

$$\sigma_{\mathsf{SI}} = \frac{\mu^2 m_{\mathsf{DM}}^2}{\pi} \cdot \frac{m_N^2}{v^2} \frac{f_N^2}{m_1^4 m_2^4} \cdot \frac{\sin^2\alpha \cos^2\alpha}{v_S^2} (m_1^2 - m_2^2)^2 \cdot \left[\frac{\mathcal{A}}{64\pi^2 v v_S^2}\right]^2 ,$$

$$\begin{aligned}\mathcal{A} =& a_1 \cdot C_2(0, m_{\mathsf{DM}}^2, m_{\mathsf{DM}}^2, m_1^2, m_2^2, m_{\mathsf{DM}}^2) + \\ & a_2 \cdot D_3(0, 0, m_{\mathsf{DM}}^2, m_{\mathsf{DM}}^2, 0, m_{\mathsf{DM}}^2, m_1^2, m_1^2, m_2^2, m_{\mathsf{DM}}^2) + \\ & a_3 \cdot D_3(0, 0, m_{\mathsf{DM}}^2, m_{\mathsf{DM}}^2, 0, m_{\mathsf{DM}}^2, m_1^2, m_2^2, m_2^2, m_{\mathsf{DM}}^2)\end{aligned}$$

with

$$\left[\frac{\mathcal{A}}{64\pi^2 v v_S^2}\right]^2 \lesssim 10^{-5}$$

In considered range of parameters, in the case of pGDM, the DD upper bound on the value of $\frac{\sin^2\alpha \cos^2\alpha}{v_S^2}(m_1^2 - m_2^2)^2$ is always higher than the value corresponding to the correct relic density (for $\sin\alpha$ that maximize the cross section for given m_2 and m_{DM}).

$$\sigma_{\mathsf{SI}} = \frac{\mu^2 m_{\mathsf{DM}}^2}{\pi} \cdot \frac{m_N^2}{v^2} \frac{f_N^2}{m_1^4 m_2^4} \cdot \frac{\sin^2\alpha \cos^2\alpha}{v_S^2} (m_1^2 - m_2^2)^2 \cdot \left[\frac{\mathcal{A}}{64\pi^2 v v_S^2}\right]^2 ,$$

The XENON1T limit for $m_{\mathsf{DM}} \gtrsim 100$ GeV can be parametrized as:

$$\frac{\sigma_{\mathsf{SI}}^{\max}}{1\ \mathsf{cm}^2} = \frac{m_{\mathsf{DM}}}{1\ \mathsf{GeV}} \cdot 10^{-48.05} .$$

Hence, the strictest possible DD limit reads

$$\frac{\sin^2\alpha \cos^2\alpha}{v_S^2} (m_1^2 - m_2^2)^2 < \frac{m_2^4}{m_{\mathsf{DM}}} \frac{v^2}{m_N^2} \frac{m_1^4}{f_N^2} \frac{\pi}{\mu^2} \frac{1\ \mathsf{cm}^2}{1\ \mathsf{GeV}} \cdot 10^{-48.05} \cdot \begin{cases} \left[\frac{\mathcal{A}}{64\pi^2 v v_S^2}\right]^{-2} & (\mathsf{pGDM}) \\ 1 & (\mathsf{FDM}, \mathsf{VDM}) \end{cases}$$

$$= \frac{m_2^4}{m_{\mathsf{DM}}} \cdot 1.5 \cdot 10^{-6}\ \mathsf{GeV}^{-1} \cdot \begin{cases} 10^5 & (\mathsf{pGDM}) \\ 1 & (\mathsf{FDM}, \mathsf{VDM}) \end{cases} .$$

Dark matter at e^+e^- colliders

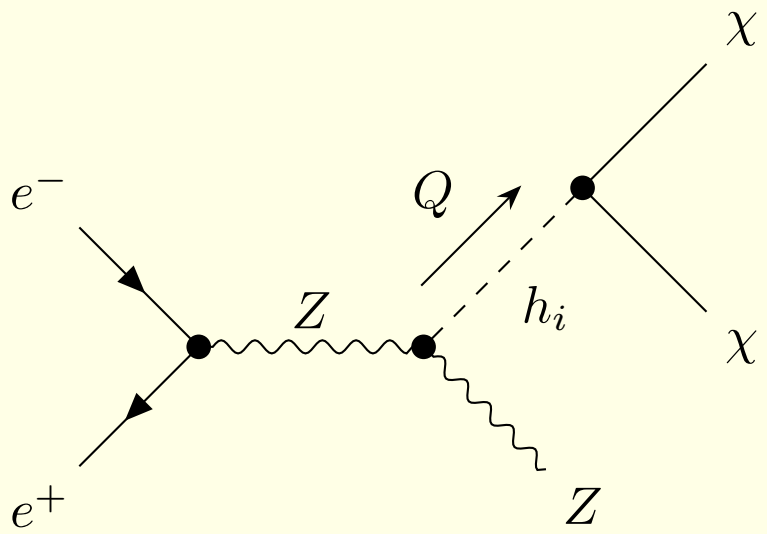

Figure 5: Feynman diagram for $e^+e^- \to Z\chi\bar{\chi}$, χ denotes the dark particle ($\chi = A, X, \psi$).

- P. Ko, H. Yokoya, "Search for Higgs portal DM at the ILC", JHEP 1608 (2016) 109,
- T. Kamon, P. Ko, J. Li "Characterizing Higgs portal dark matter models at the ILC", Eur.Phys.J. C77 (2017) no.9, 652

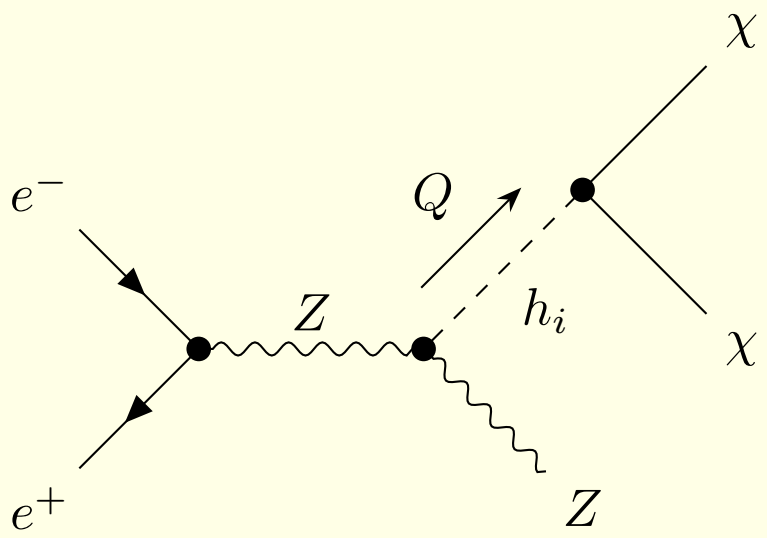

Figure 6: Feynman diagram for $e^+e^- \to Z\chi\bar{\chi}$, χ denotes the dark particle ($\chi = A, X, \psi$).

$$\frac{d\sigma}{dQ^2}(Q^2) = \frac{f(s,\sqrt{Q^2})}{32\pi^2} \frac{\left(Q^2\right)^2 \cdot \sin^2\alpha \cos^2\alpha \cdot \left[(m_1^2 - m_2^2)^2 + (m_1\Gamma_1 - m_2\Gamma_2)^2\right]}{\left[(Q^2 - m_1^2)^2 + (m_1\Gamma_1)^2\right]\left[(Q^2 - m_2^2)^2 + (m_2\Gamma_2)^2\right]} \times$$

$$\times \sqrt{1 - 4\frac{m_{\mathsf{DM}}^2}{Q^2}} \cdot \frac{1}{v_S^2} \cdot \begin{cases} 1 & (\mathsf{pGDM}) \\ 1 - 4\frac{m_{\mathsf{DM}}^2}{Q^2} + 12\left(\frac{m_{\mathsf{DM}}^2}{Q^2}\right)^2 & (\mathsf{VDM}) \\ 2\left[\frac{m_{\mathsf{DM}}^2}{Q^2} - 4(\frac{m_{\mathsf{DM}}^2}{Q^2})^2\right] & (\mathsf{FDM}) \end{cases}$$

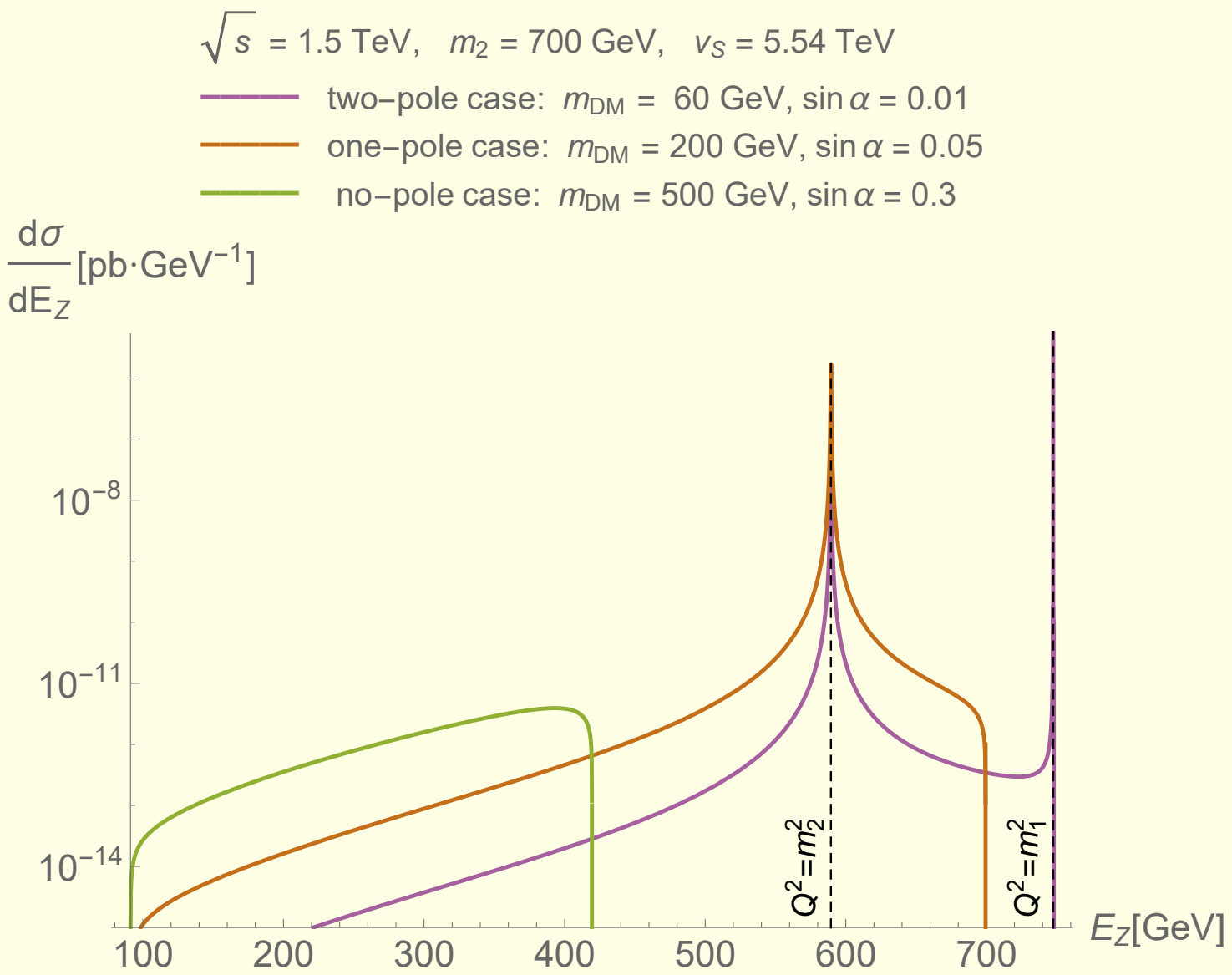

Figure 7: $\frac{d\sigma}{dE_Z}$ for the pGDM model.

$$E_Z(Q^2 = m_i^2) = E_i \equiv \frac{s - m_i^2 + m_Z^2}{2\sqrt{s}}, \qquad E_{\max} = \frac{s - 4m_{DM}^2 + m_Z^2}{2\sqrt{s}}$$

Background

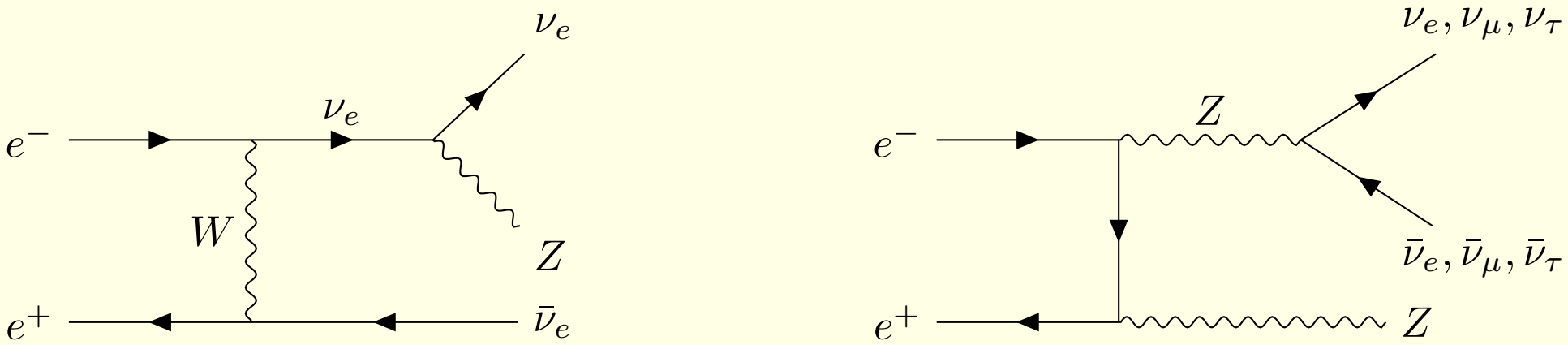

Figure 8: Exemplary diagrams of the Standard Model background processes. Neutrinos contribute to missing energy and can therefore mimic dark particles. The background cross-section could be reduced by polarizing the initial e^+ and e^- beams.

Strategy

- Fix $\sqrt{s}$ e.g. at 240 GeV for the CEPC, or $\sqrt{s} = 250$ GeV for the ILC,

- Parameters: m_2, m_{DM}, $\sin\alpha$ and v_S,

- For given (m_2, m_{DM}) and $\sin\alpha$, the value of v_S is derived by solving the relic-density condition, so v_S is no longer independent:

$$\frac{\sin^2\alpha\cos^2\alpha}{v_S^2}(m_1^2 - m_2^2)^2 =$$

$$= 2.1\cdot 10^{-5}\ \mathsf{GeV}^{-2}\frac{(m_1^2 - 4m_{\mathsf{DM}}^2)^2\,(m_2^2 - 4m_{\mathsf{DM}}^2)^2}{m_{\mathsf{DM}}(m_{\mathsf{DM}}^2 - m_b^2)^{3/2}}\cdot\begin{cases}\frac{1}{12} & (\mathsf{pGDM})\\ 1 & (\mathsf{VDM})\\ \frac{4m_{DM}}{9T_f} & (\mathsf{FDM})\end{cases}$$

- For each point (m_2, m_{DM}) of the plot, we choose such value of $\sin\alpha \leq 0.3$ that maximizes the total cross section.

Extra scalars at 500 ILC → Exclusion Limits

Prelimiary results for 500 GeV.

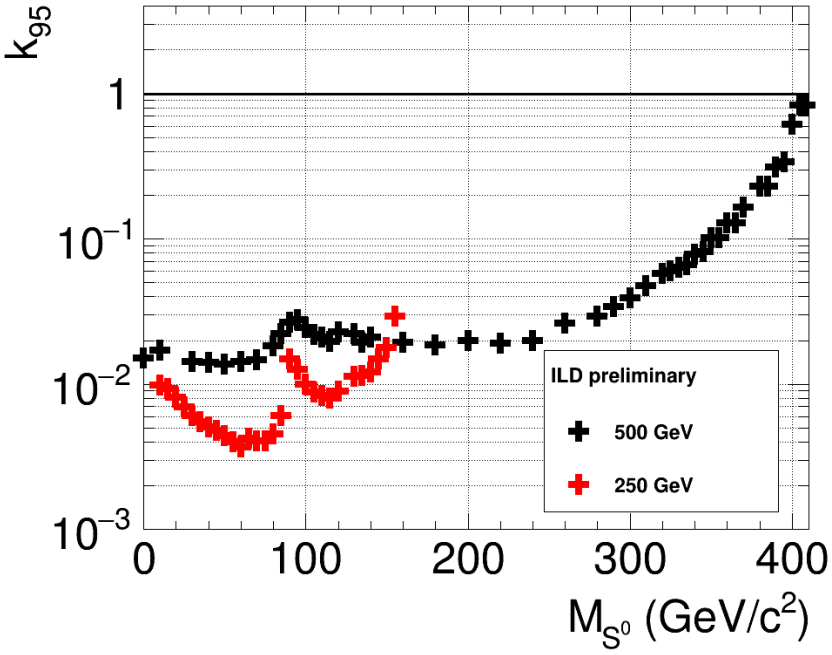

Figure 9: Expected sensitivity for the measurement of the cross-section for $e^+e^- \to DM\,DM\,Z$ at the ILC, from Yan Wang (DESY, IHEP) at LCWS 2018, Arlington, October 25, 2018. $\kappa_{95} \equiv \sigma(e^+e^- \to \cdots + Z)/\sigma_{SM}(e^+e^- \to h_{SM}Z)$

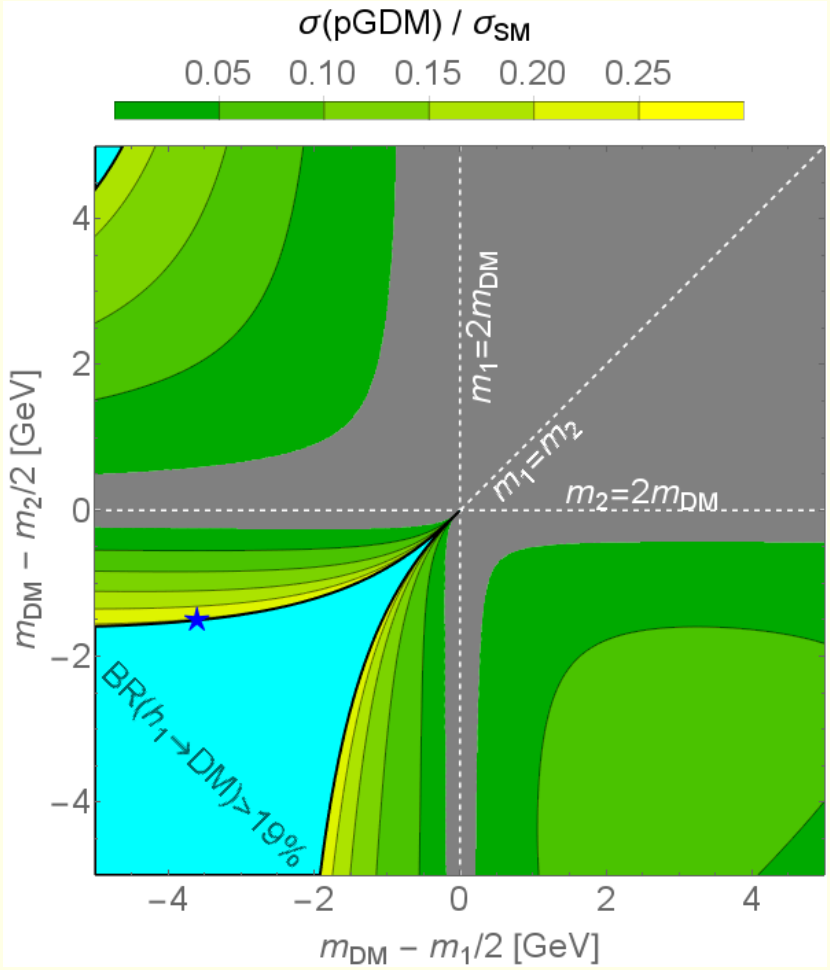

benchmark point for pGDM

$m_2 = 120.8$ GeV , $m_{\text{DM}} = 58.9$ GeV ,

$\sin\alpha = 0.30$, $v_S = 646$ GeV ,

$\Gamma_1 = 7.4 \cdot 10^{-3}$ GeV , $\Gamma_2 = 9.8 \cdot 10^{-3}$ GeV ,

$\text{BR}(h_1 \to \text{DM}) = 19\%$, $\text{BR}(h_2 \to \text{DM}) = 95\%$,

$\sigma = 62$ fb

Figure 10: For the pGDM, the allowed region (greenish), the region forbidden by the invisible BR of h_1 (cyan) where $\text{BR}(h_1 \to \text{DM}) > 19\%$ and the gray region where the cross section falls below its expected precision at the 95% CL. Coloring of the greenish area shows the value of the normalized total cross section σ/σ_{SM}. The star denotes the chosen benchmark point, characterized by relatively high cross section.

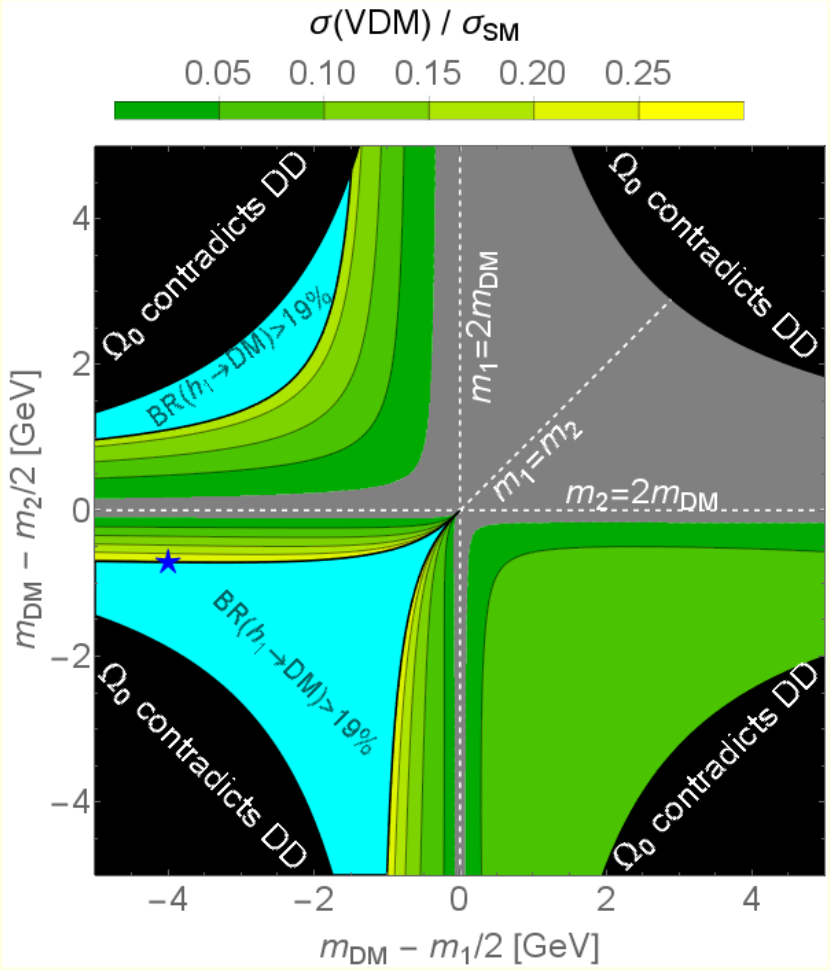

benchmark point for VDM

$m_2 = 118.4$ GeV , $m_{\text{DM}} = 58.5$ GeV ,

$\sin\alpha = 0.30$, $v_S = 561$ GeV ,

$\Gamma_1 = 7.4 \cdot 10^{-3}$ GeV , $\Gamma_2 = 6.4 \cdot 10^{-3}$ GeV ,

$\text{BR}(h_1 \to \text{DM}) = 18\%$, $\text{BR}(h_2 \to \text{DM}) = 92\%$,

$\sigma = 61$ fb

Figure 11: As in Fig. 10 for the VDM model. The region forbidden by the DD constraint is denoted in black.

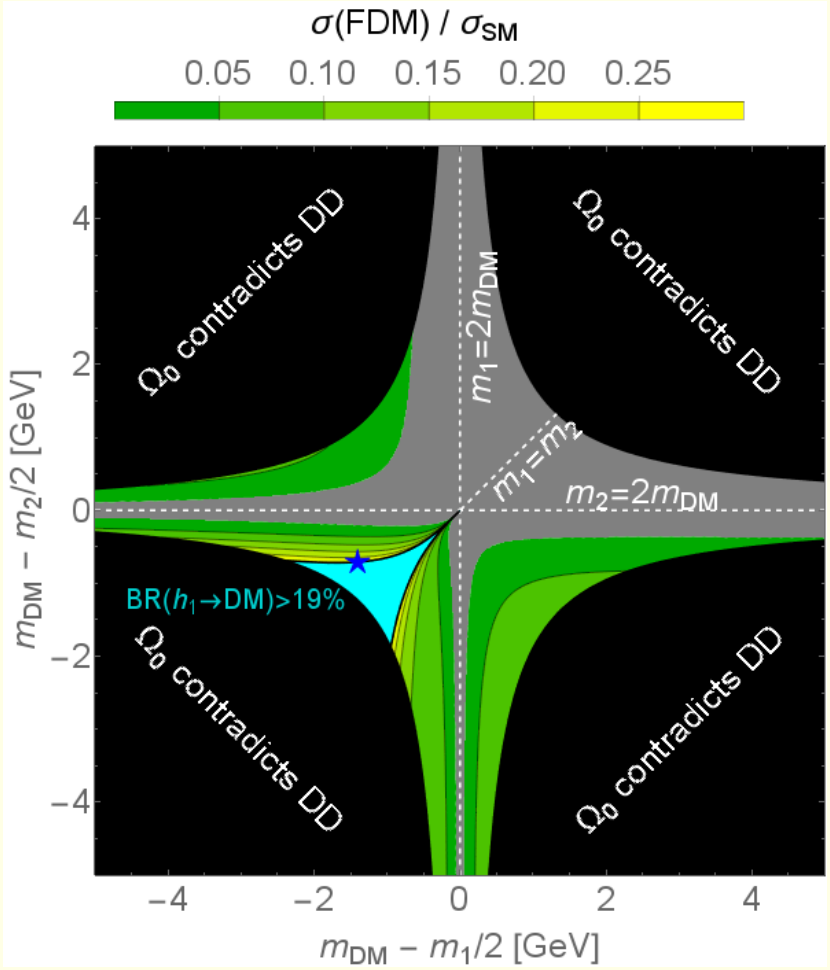

benchmark point for FDM

$m_2 = 123.6$ GeV , $m_{\text{DM}} = 61.1$ GeV ,

$\sin\alpha = 0.30$, $v_S = 76$ GeV ,

$\Gamma_1 = 7.4 \cdot 10^{-3}$ GeV , $\Gamma_2 = 5.9 \cdot 10^{-3}$ GeV ,

$\text{BR}(h_1 \to \text{DM}) = 18\%$, $\text{BR}(h_2 \to \text{DM}) = 91\%$,

$\sigma = 59$ fb

Figure 12: As in Fig. 10 for the FDM model. The region forbidden by the DD constraint is denoted by black.

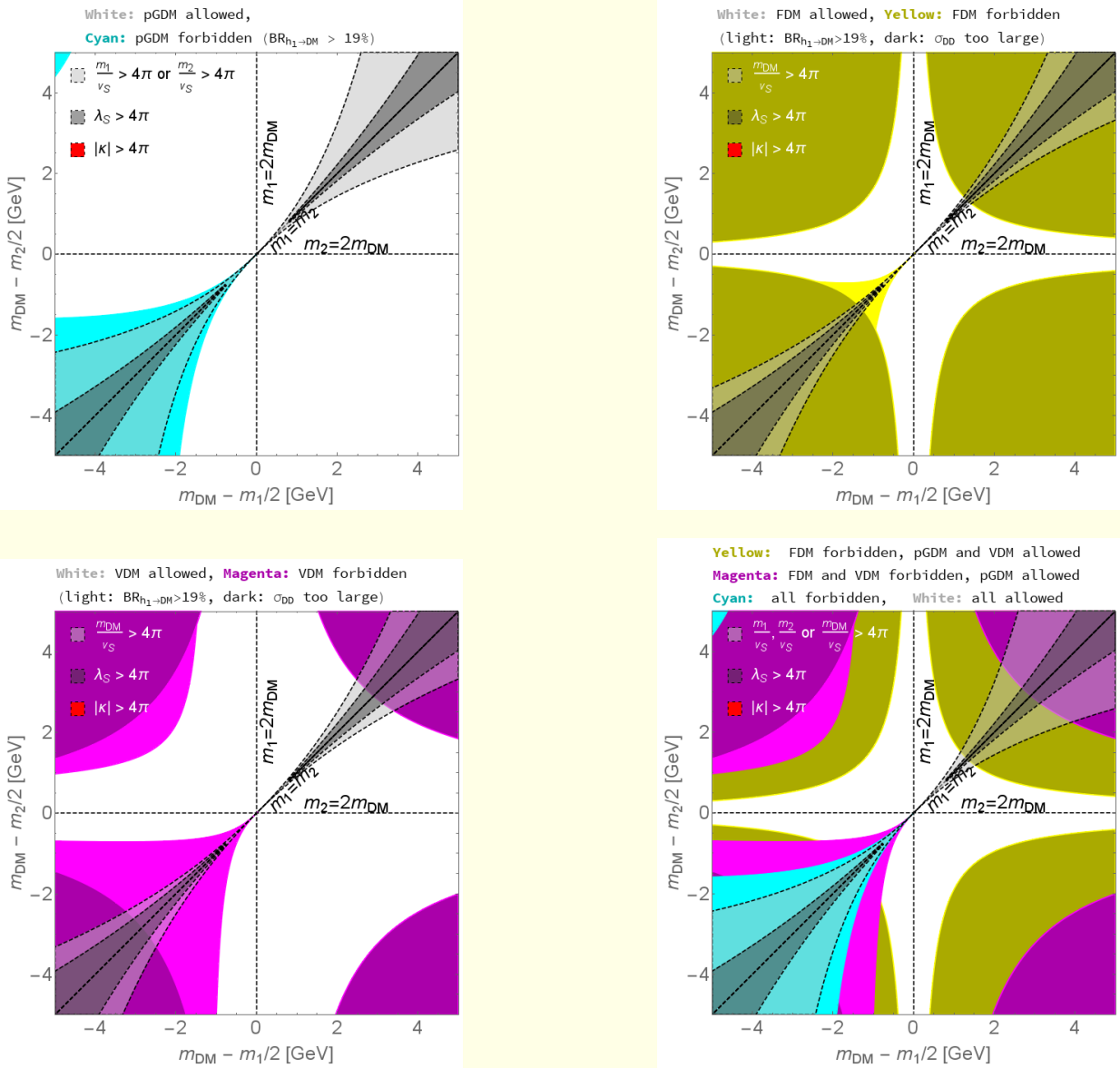

Figure 13: Top-left: pGDM model, top-right: FDM model, bottom-left: VDM model, bottom-right: the three models combined. Light- and dark-gray regions denote violation of perturbativity conditions. Note that the $|\kappa| < 4\pi$ condition is not violated in any place of the considered range of parameters.

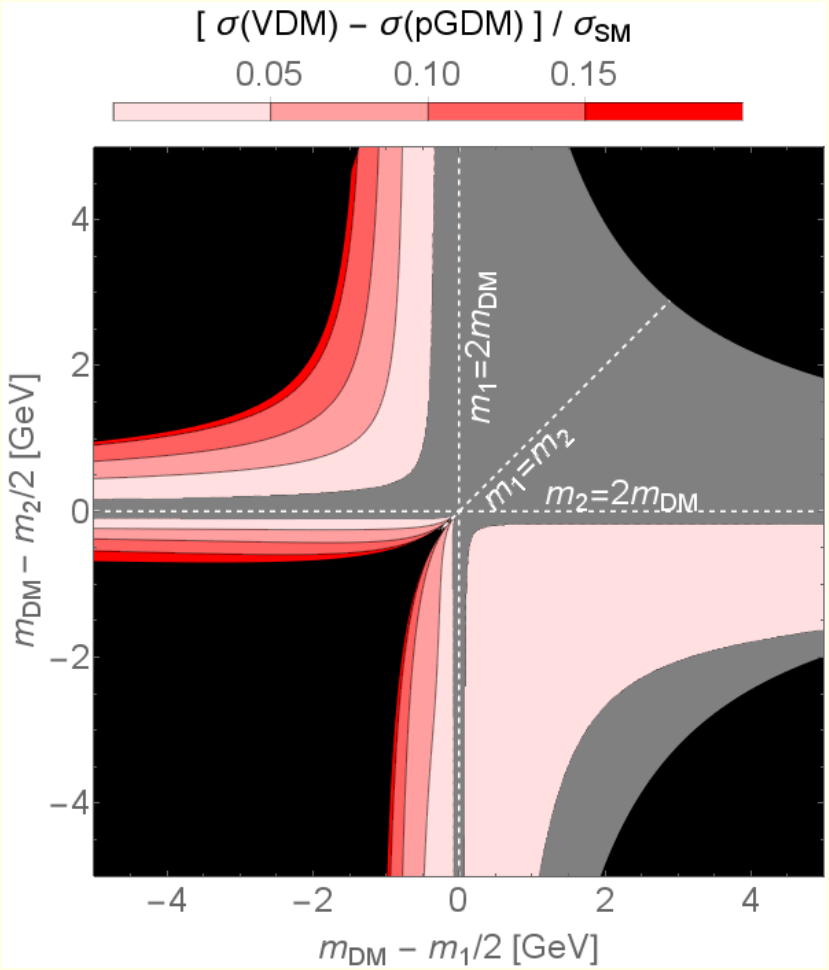

Figure 14: The difference between predictions for the pGDM and the VDM. The gray region denotes parameter space for which the difference is smaller than the limit of Fig. 9. The models are compared in the region where both of them are consistent with the data, see Fig. 13.

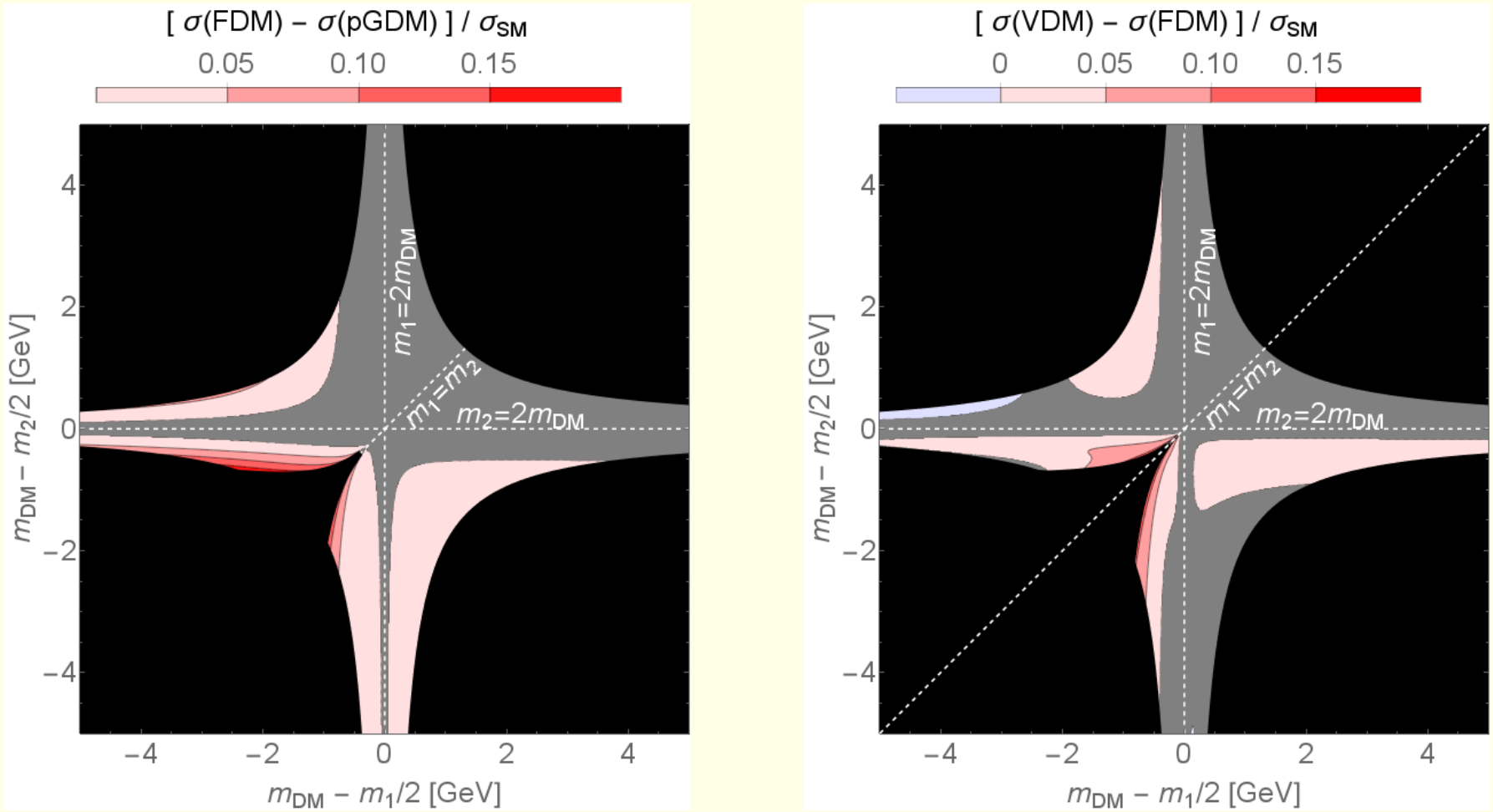

Figure 15: The difference between predictions for the pGDM and the FDM (left panel), and the FDM and the VDM (right panel). The gray region denotes parameter space for which the difference is smaller than the limit of Fig. 9. The models are compared in the region where both of them are consistent with the data, see Fig. 13.

Summary

1. The following models were discussed and compared:
   - pGDM with complex scalar field S and $U(1)$ global symmetry softly broken by $\mu^2(S^2 + S^{*\,2})$,
   - VDM with gauged $U(1)_X$ and complex S,
   - FDM with chiral χ and real S.

2. Perturbativity, vacuum stability and globality of the vacuum ensured.

3. - Limits for invisible Higgs boson decays $BR(h_1 \to DM\ \ DM) < 19\%$ and LHC limits on $\sin\alpha < 0.30$ imposed.
   - Limits from ID and DD satisfied.
   - DM abundance constraint satisfied.

4. Direct detection efficiently suppressed in the pGDM model, $\sigma_{\mathsf{SI}} \propto v_A^4$, as a consequence of A being a pseudo-Goldstone boson, 1-loop calculations were performed and adopted. For $q^2 = 0$ the 1-loop results are UV finite and vanish in the limit $m_A = m_{DM} \to 0$.

5. In some regions of (m_2, m_{DM}) space e^+e^- colliders might be useful to disentangle the models.

Backup slides: Vacuum stability

$$V_{\rm VDM}(H,S) = -\mu_H^2|H|^2 + \lambda_H|H|^4 - \mu_S^2|S|^2 + \lambda_S|S|^4 + \kappa|S|^2|H|^2$$

$$\lambda_H(Q) > 0, \quad \lambda_S(Q) > 0, \quad \kappa(Q) + 2\sqrt{\lambda_H(Q)\lambda_S(Q)} > 0$$

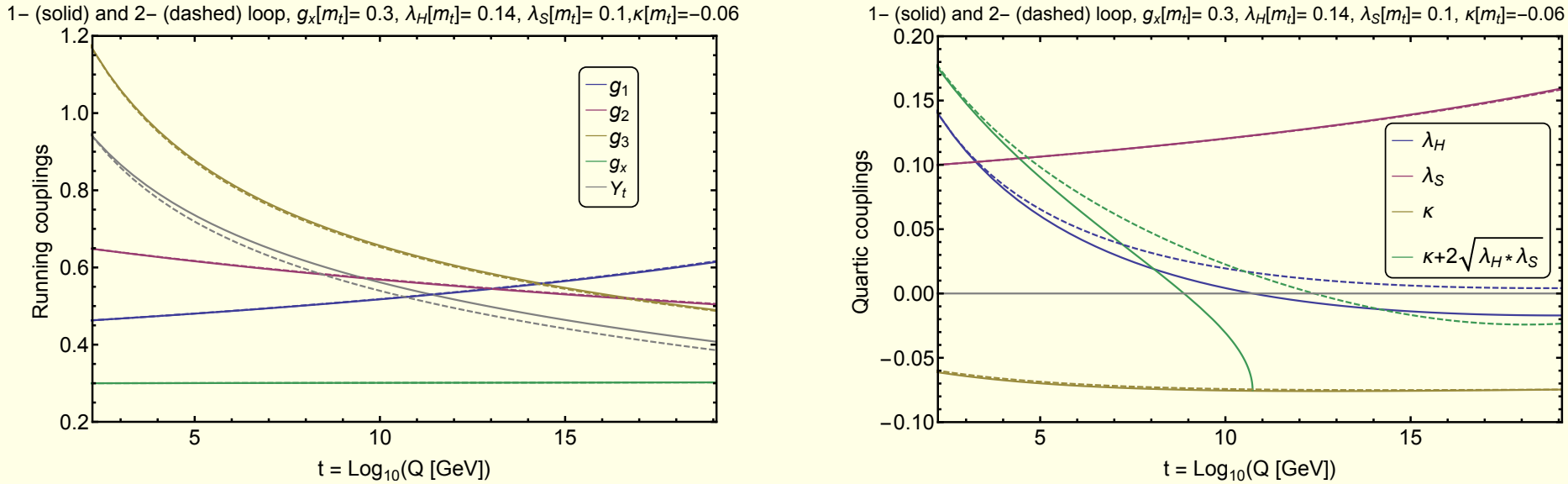

Figure 16: Running of various parameters at 1- and 2-loop, in solid and dashed lines respectively. For this choice of parameters $\lambda_H(Q) > 0$ at 2-loop (right panel blue) but not at 1-loop. $\lambda_S(Q)$ is always positive (right panel red), running of $\kappa(Q)$ is very limited, however the third positivity condition $\kappa(Q) + 2\sqrt{\lambda_H(Q)\lambda_S(Q)} > 0$ is violated at higher scales even at 2-loops (right panel green).

The mass of the Higgs boson is known experimentally therefore within $the\ SM$ the initial condition for running of $\lambda_H(Q)$ is fixed

$$\lambda_H(m_t) = M_{h_1}^2/(2v^2) = \lambda_{SM} = 0.13$$

For VDM this is not necessarily the case:

$$M_{h_1}^2 = \lambda_H v^2 + \lambda_S v_S^2 \pm \sqrt{\lambda_S^2 v_S^4 - 2\lambda_H \lambda_S v^2 v_S^2 + \lambda_H^2 v^4 + \kappa^2 v^2 v_S^4}.$$

VDM:

- Larger initial values of λ_H such that $\lambda_H(m_t) > \lambda_{SM}$ are allowed delaying the instability (by shifting up the scale at which $\lambda_H(Q) < 0$).

- Even if the initial λ_H is smaller than its SM value, $\lambda_H(m_t) < \lambda_{SM}$, still there is a chance to lift the instability scale if appropriate initial value of the portal coupling $\kappa(m_t)$ is chosen.

$$\beta_{\lambda_H}^{(1)} = \beta_{\lambda_H}^{SM\ (1)} + \kappa^2$$

$$f(s,\sqrt{Q^2}) \equiv \frac{g_V^2+g_A^2}{24\pi}\left(\frac{g^2}{\cos\theta_W^2}\frac{1}{s-m_Z^2}\right)^2 \frac{\lambda^{1/2}(s,Q^2,m_Z^2)\left[12\,s\,m_Z^2+\lambda(s,Q^2,m_Z^2)\right]}{8s^2}$$

$$Q^2 = Q^2(s,E_Z) \equiv s - 2E_Z\sqrt{s} + m_Z^2$$

$$E_Z(Q^2=m_i^2) = E_i \equiv \frac{s-m_i^2+m_Z^2}{2\sqrt{s}}.$$

$$E_{\rm max} = \frac{s-4m_{DM}^2+m_Z^2}{2\sqrt{s}},$$